

BIFURCATIONS AND CHAOS IN MODELS OF SPACECRAFT POWER SYSTEMS

Yan Hong Lim and David C. Hamill

Surrey Space Centre
University of Surrey, Guildford, Surrey GU2 5XH, UK
Tel. +44 (0) 1483 259278, Fax +44 (0) 1483 259503
 Email: Y.Lim@surrey.ac.uk, D.Hamill@surrey.ac.uk

Abstract — We describe the recent application of nonlinear-dynamics theory and techniques to spacecraft power systems. We study several simple models, which reveal a variety of bifurcations, coexisting attractors and chaotic behaviour.

I. INTRODUCTION

Direct-current (dc) power systems are universally used in small spacecraft such as satellites. Dc power is generated by solar arrays, batteries are used as energy reservoirs, and the payloads need dc supplies.

Dc power systems and the power-electronic circuits incorporated within them are nonlinear. Besides the power converters, which are nonlinear dynamical systems in their own right, even the usual power sources and loads have inherently nonlinear characteristics. The result can be unpredictable and erratic behaviour. When this surfaces in a mode of operation assumed to be stable, the unwary engineer often dismisses it as interference, noise, faulty components, bad connections, and so on. This is because system models and analysis are usually based on simple linear techniques; unsurprisingly, these fail to predict essentially nonlinear phenomena.

This was effectively revealed in [1], where a simple dc-dc converter was analysed using conventional linear methods and nonlinear methods [2]. The linear analysis indicated stability over a wide input-voltage range, while the nonlinear treatment revealed a wide range of nonlinear behaviour, which has been verified experimentally. Although some nonlinear effects may be merely undesirable, others can have a catastrophic impact. For example, chattering (an uncontrolled increase in switching frequency) can elevate switching losses to a destructive level in a dc-dc converter.

With an abundance of nonlinearity and the ever-increasing complexity of system architecture to satisfy power and reliability requirements, it is very likely that hidden anomalies could remain undiscovered in spacecraft power systems. This has important implications in a field where high reliability is essential.

Nonlinear dynamics has been applied to terrestrial alternating-current power systems to explain unforeseen loss of steady-state stability, voltage collapse and asynchronous oscillations [3–5]. But there has been little work in the field of dc power systems. A simple model spacecraft power system was studied by other workers, using state-plane analysis techniques [6]. That work was based on a second-order nonlinear model comprising a solar array, a filter, and a dc-dc converter load. The existence of multiple equilibrium points was demonstrated, and their stability established.

Because spacecraft power systems are complex, our work has begun by investigating simplified but relevant models. We hope to understand some of the nonlinear dynamics involved, and subsequently use the techniques to improve the design of real space power systems.

II. HYSTERESIS IN A FIRST-ORDER SYSTEM

Consider the simple first-order system of Fig. 1. A solar array feeds power to the payload, R_L , via a reservoir capacitor C and a model of a buck dc-dc converter. A satellite in space experiences various degrees of illumination and changing payload power requirements. The solar array's terminal voltage v_1 and current i_1 vary in response to these changes but are constrained to lie within its open circuit voltage V_{oc} and short circuit current I_{sc} respectively. Throughout this paper, we use the coefficient α to denote the relative solar illumination ($0 \leq \alpha \leq 1$) and use it as our chief bifurcation parameter.

We can approximate the dc characteristics of a solar array by the polynomial

$$i_1 = \alpha I_{sc} \left(1 - \left(\frac{v_1}{V_{oc}} \right)^p \right) \quad 0 \leq v_1 \leq V_{oc}, \quad 0 \leq i_1 \leq I_{sc} \quad (1)$$

where $p = 33$ is chosen to match real solar arrays.

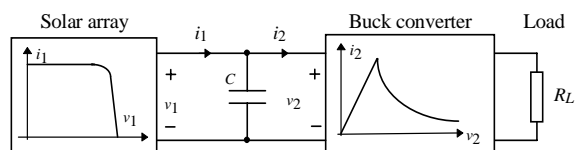


Figure 1: Schematic of a first-order power system

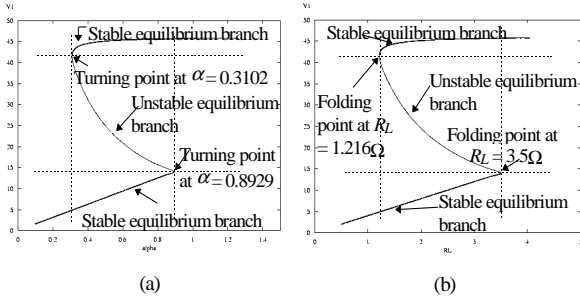


Figure 2: (a) Bifurcation diagram of v_1 against α , showing hysteresis for $0.3102 < \alpha < 0.8929$; (b) bifurcation diagram of v_1 against R_L , showing hysteresis for $1.126\Omega < R_L < 3.5\Omega$

Because the array voltage varies, there are two modes of dc-dc converter operation. One is desirable, the other undesirable. The buck converter's role is to maintain a constant voltage across R_L . With sufficient voltage from the solar array, the output is regulated and constant, resulting in a constant-power input characteristic. However, when there is insufficient voltage, it operates in the undesirable mode, where the output is not regulated and there is a constant-resistance input characteristic. Overall,

$$i_2 = \begin{cases} \frac{V_{ref}^2}{R_L v_2} & \text{if } v_2 \geq V_{ref} \quad (\text{desirable mode}) \\ \frac{v_2}{R_L} & \text{if } v_2 < V_{ref} \quad (\text{undesirable mode}) \end{cases} \quad (2)$$

where i_2 and v_2 are the input current and voltage and V_{ref} is the desired output voltage. Since $v_2 = v_1$, the system equation is

$$\frac{dv_1}{dt} = \frac{i_1(v_1) - i_2(v_1)}{C} \quad (3)$$

The following parameter values were used: $I_{sc} = 4A$, $V_{oc} = 46.2V$, $V_{ref} = 14V$, $C = 250\mu F$, with nominal values of $R_L = 3.92\Omega$ and $\alpha = 1$. We used standard packages [7, 8] to generate the bifurcation diagrams of Fig. 2 for parameters α and R_L . In each case, there is an interval of parameter values where two values of array voltage are stable and one is unstable. At the extremes of this range, a pair of equilibria merge and vanish, resulting in a saddle-node bifurcation. This is well known as hysteresis.

We can see how this happens graphically in Fig. 3, where the solar array's dc characteristic and the converter's are superimposed. At a high illumination α_1 , there is a single, stable equilibrium (point D). When the illumina-

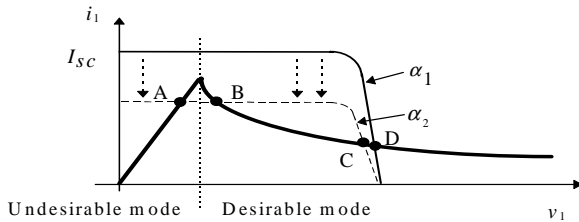


Figure 3: V - I characteristics, showing equilibrium points A, B, C and D

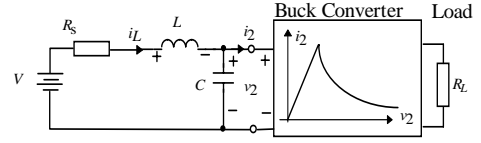


Figure 4: Voltage source coupled via second order filter to dc-dc converter

tion decreases to α_2 , D moves to C. However, two additional equilibria emerge, A (stable) and B (unstable). A large perturbation (due to a momentary drop in illumination or a load power surge, say) might propel the system to A, a stable but undesirable equilibrium. This is known as *voltage collapse* — a notorious hazard of spacecraft power-system operation, which results in temporary loss of the satellite's functions. For example, in a direct-broadcast satellite, tv programmes might be interrupted. To escape from it and return to the desirable stable equilibrium C, either the illumination has to be restored to an adequate level, or payloads have to be switched off — an operation known as *load shedding*.

III. HOPF BIFURCATION IN SECOND AND THIRD-ORDER SYSTEMS

A. Second-Order System

In our next example (Fig. 4), we take a voltage source with internal resistance, and couple it via a second-order filter to the dc-dc converter. (In a real power system, such a filter is used to reduce the ripple current flowing from the converter back to the main power bus.) We use the following parameter values: $V = 25V$, $L = 250\mu H$, $C = 120\mu F$, $R_s = 0.2\Omega$, retaining the previous parameters for the dc-dc converter.

In circuit terms, self-oscillation arises from the negative input resistance of the converter, a well known effect. However, conventional linear analysis gives misleading results. Let the instantaneous values of i_2 and v_2 be

$$i_2 = I_2 + \hat{i}_2 \quad (4)$$

$$v_2 = V_2 + \hat{v}_2 \quad (5)$$

where I_2 , V_2 are the equilibrium values and \hat{i}_2 , \hat{v}_2 are small perturbations. In the steady state,

$$V - i_2 R_s = V_2 \quad (6)$$

Substituting (4) and (5) into (2),

$$I_2 + \hat{i}_2 = \frac{V_{ref}^2}{R_L V_2} \left(1 + \frac{\hat{v}_2}{V_2}\right)^{-1} \approx \frac{V_{ref}^2}{R_L V_2} \left(1 - \frac{\hat{v}_2}{V_2}\right) \quad (7)$$

Equating the constant and perturbation terms and substituting (6) into (7), we find

$$V_2 = \frac{V}{2} + \sqrt{\frac{V^2}{4} - \frac{R_s V_{ref}^2}{R_L V}} \quad (8)$$

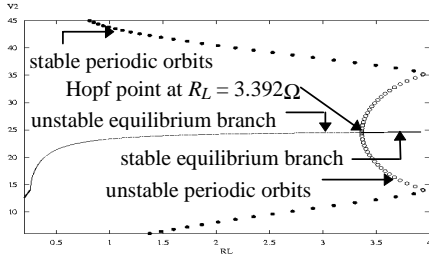


Figure 5: Bifurcation diagram of v_2 against R_L showing subcritical Hopf bifurcation

$$\text{and } r_2 = \frac{\hat{v}_2}{\hat{i}_2} = -\left(\frac{V_2}{V_{ref}}\right)^2 R_L \quad (9)$$

This linearised dynamic resistance is negative. The output admittance of the voltage source–filter combination can be found as

$$Y = \frac{R_s}{R_s^2 + \omega^2 L^2} + j \frac{\omega^3 L^2 C + \omega(CR_s^2 - L)}{R_s^2 + \omega^2 L^2} = G + jB \quad (10)$$

For sustained oscillation, $1/r_2 + G = 0$ and $B = 0$, giving two expressions for ω . Equating them, we find

$$r_2 = -\frac{L}{CR_s} \quad (11)$$

With the parameter values chosen, (11) is satisfied when $R_L = 3.39\Omega$. For this condition the linearised circuit becomes Hamiltonian.

Let us compare this with a nonlinear analysis. Using R_L as the bifurcation parameter (Fig. 5), we observe a subcritical Hopf bifurcation at $R_L = 3.39\Omega$, which result in both unstable periodic orbits (denoted by open dots) and stable limit cycles (filled dots). The subcritical Hopf bifurcation occurs where a stable equilibrium and an unstable periodic orbit meet.

Both analyses predict oscillation for $R_L \leq 3.39\Omega$ and a stable equilibrium for $R_L > 3.39\Omega$. However, the nonlinear analysis reveals that for $3.39\Omega < R_L < 3.97\Omega$, a stable equilibrium coexists with a limit cycle. Under a large enough perturbation, the system could break into oscillation, which might cause malfunction or damage. The conventional linear analysis misses this possibility.

B. Third-Order System

As a third example, we extend the model to include the solar array characteristics (Fig. 6), and add a further capacitor, making the system third-order. Here, $C_1 = 50\mu\text{F}$, $C_2 = 350\mu\text{F}$ and $L = 700\mu\text{H}$. The system equations are

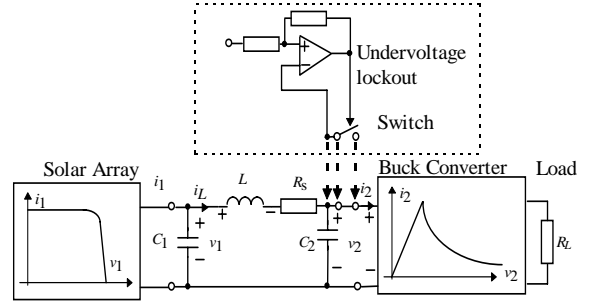


Figure 6: Schematic of power system including third-order filter and showing the inclusion of an undervoltage lockout circuit

$$\left. \begin{aligned} \frac{dv_1}{dt} &= \frac{i_1(v_1) - i_L}{C_1} \\ \frac{di_L}{dt} &= \frac{v_1 - i_L R_s - v_2}{L} \\ \frac{dv_2}{dt} &= \frac{i_L - i_2(v_2)}{C_2} \end{aligned} \right\} \quad (12)$$

From the bifurcation diagram of Fig. 7, we again find hysteresis and Hopf bifurcation, leading to limit cycles and coexisting attractors.

IV. COEXISTING LIMIT CYCLES AND CHAOS

Finally, we add an undervoltage lockout to the converter of Fig. 6. When v_2 falls below a preset threshold (here 19V), the switch opens and disconnects the converter's input. The switch remains open until the input voltage rises above a higher preset threshold (here 21V); then the switch closes and reconnects the converter. (Hysteresis is incorporated to prevent chattering.) Such circuits are commonly employed in space power systems to avoid overdischarging the batteries during eclipse, and to ensure that converters operate in their proper mode so payloads receive a regulated voltage or no supply at all. In

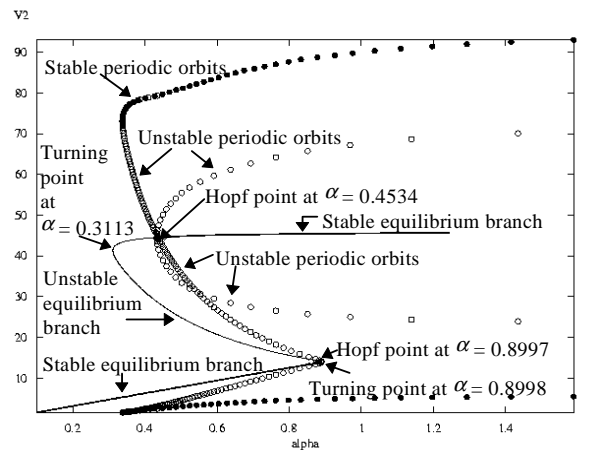


Figure 7: Bifurcation diagram of v_2 against α showing hysteresis between $0.3113 < \alpha < 0.8998$, two Hopf points at $\alpha = 0.3434$ and $\alpha = 0.8997$, where subcritical Hopf bifurcations occur. Filled dots represent stable periodic orbits; open dots represent unstable periodic orbits

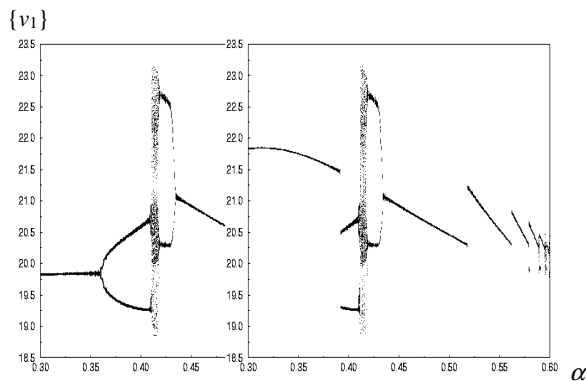


Figure 8: Bifurcation diagram of $\{v_1\}$ against α with different initial conditions; left: $v_1 = 20\text{V}$, $i_L = 1\text{A}$, $v_2 = 20\text{V}$, right: $v_1 = 20.9\text{V}$, $i_L = 1\text{A}$, $v_2 = 20.9\text{V}$

our model, $L = 250\mu\text{H}$, $C_1 = 120\mu\text{F}$, $C_2 = 250\mu\text{F}$ and $R_s = 0.2\Omega$.

Fig. 8 shows bifurcation diagrams of $\{v_1\}$ against α , obtained from a Poincaré section at $v_2 = 21\text{V}$. Two diagrams were computed using different initial conditions. From $\alpha = 0.30$ to 0.36 two limit cycles coexist (see Fig. 9), each with its own basin of attraction. At $\alpha = 0.32$, the outer cycle has a period of 1.28ms and the inner cycle a period of 0.64ms . At $\alpha = 0.36$, the inner limit cycle period-doubles. At $\alpha = 0.39$, the two limit cycles collide, and the inner (period-2) one dominates; from here on, the two bifurcation diagrams are identical. At $\alpha = 0.41$ the period-2 orbit explodes into chaos, lasting until $\alpha = 0.42$.

At $\alpha = 0.415$, simulations repeated with initial conditions differing by just 0.01V showed trajectories rapidly diverging from each other, exhibiting sensitive dependence on initial condition. The Poincaré map of Fig. 10 was constructed by plotting v_1 against i_L , sampled at $v_2 = 20\text{V}$. The fractal nature of the attractor is further evidence of chaos.

Period-2 re-emerges at $\alpha = 0.42$, converging to period-1 at $\alpha = 0.43$. As α is increased further, discontinuities are witnessed. They arise from the convenient choice of $v_2 = 21\text{V}$ (equal to the upper hysteresis threshold) as the Poincaré section, which is just touched every cycle. Actually, period multiplication is taking place; it would be more

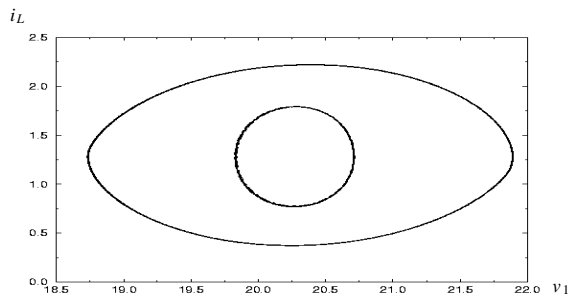


Figure 9: Coexisting limit cycles. Initial conditions for inner cycle: $v_1 = 20\text{V}$, $i_L = 1\text{A}$, $v_2 = 20\text{V}$; for outer cycle: $v_1 = 20.9\text{V}$, $i_L = 1\text{A}$, $v_2 = 20.9\text{V}$

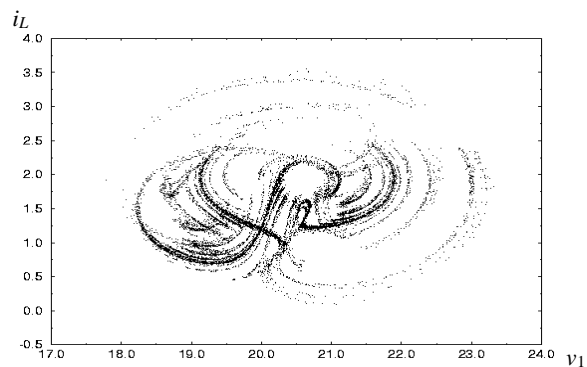


Figure 10: Poincaré mapping sectioned at $v_2 = 20\text{V}$, for $\alpha = 0.415$

obvious with a different choice of section (e.g. $v_2 = 20\text{V}$). At each discontinuity, there is evidence of a narrow band of chaos (possibly a chaotic transient). With adequate illumination ($\alpha > 0.6$), the switch closes continuously and operation reverts to a stable equilibrium.

V. CONCLUSION

Various aspects of spacecraft power system stability have been studied with the aid of simplified models. Both analytical and numerical methods were applied. The results include hysteresis, Hopf bifurcation, period multiplication, coexisting attractors and chaos. This continuing work has important implications for the performance and reliability of real spacecraft power systems.

REFERENCES

- [1] D.C. Hamill, "Power electronics: a field rich in nonlinear dynamics", *Workshop Nonlinear Dynamics of Electronic Systems*, Dublin, pp.164–179, July 1995
- [2] D.C. Hamill, J.H.B. Deane and D.J. Jefferies, "Modeling of chaotic dc-dc converters by iterated nonlinear mappings", *IEEE Trans. on Power Electronics*, vol. 7, no. 1, pp. 25-36, Jan. 1992
- [3] H.G. Kwantny, A.K. Pasrija and L.Y. Bahar, "Static bifurcations in electric power networks: loss of steady-state stability and voltage collapse", *IEEE Trans. on Circuits and Systems*, vol. 33, no. 10, pp. 981-991, Oct. 1986
- [4] H.D. Chiang, C.W. Liu, P.P. Varaiya, F.F. Wu and M.G. Lauby, "Chaos in a simple power system", *IEEE Trans. on Power Systems*, vol. 8, no. 4, pp. 1407-1417, Nov. 1993
- [5] H.O. Wang, E.H. Abed and A.M.A. Hamdan, "Bifurcations, chaos, and crises in voltage collapse of a model power system", *IEEE Trans. on Circuits and Systems*, Part I, vol. 41, no. 4, pp. 294-302, Mar. 1994
- [6] B.H. Cho, J. R. Lee and F.C. Lee, "Large-signal stability analysis of spacecraft power processing systems", *Power Electronics Specialists Conf.*, pp. 289-294, 1987
- [7] B. Ermentrout, *XPPAUT*, Univ. of Pittsburg (<http://www.pitt.edu/~phase/>)
- [8] E. Doedel, *AUTO*, Concordia Univ.

(<ftp://ftp.cs.concordia.ca/pub/doedel/auto/>)